# Sensitivity of vortex pairing and mixing to initial perturbations in stratified shear flows

Wenjing Dong,[1] E. W. Tedford,[1] M. Rahmani,[2] and G. A. Lawrence[1]
[1]*Department of Civil Engineering, University of British Columbia, Vancouver, BC V6T 1Z4, Canada*
[2]*Department of Mathematics, University of British Columbia, Vancouver, BC V6T 1Z2, Canada*

(Received 30 November 2018; published 7 June 2019)

The effects of different initial perturbations on the evolution of stratified shear flows that are subject to Kelvin-Helmholtz instability and vortex pairing have been investigated through direct numerical simulation. The effects of purely random perturbations of the background flow are sensitive to the phase of the subharmonic component of the perturbation that has a wavelength double that of the Kelvin-Helmholtz instability. If the phase relationship between the Kelvin-Helmholtz mode and its subharmonic mode is optimal, or close to it, then vortex pairing occurs. Vortex pairing is delayed when there is a phase difference, and this delay increases with increasing phase difference. In three-dimensional simulations vortex pairing is suppressed if the phase difference is sufficiently large, reducing the amount of mixing and mixing efficiency. For a given phase difference close enough to the optimal phase, the response of the flow to eigenfunctions perturbations is very similar to the response to random perturbations. The phase difference has a more significant effect on vortex pairing compared to the initial perturbation amplitude ratio between the KH and the subharmonic modes. In addition to traditional diagnostics, we show quantitatively that a nonmodal Fourier component in a random perturbation quickly evolves to be modal and describe the process of vortex pairing using Lagrangian trajectories.

DOI: 10.1103/PhysRevFluids.4.063902

## I. INTRODUCTION

Fluids are often stably stratified in the atmosphere, ocean, and lakes, due to temperature or salinity or both. The existence of shear (vertical variations in the horizontal currents) may give rise to instabilities in these otherwise stably stratified flows. Kelvin-Helmholtz (KH) instabilities, also called Rayleigh instabilities in homogeneous fluids, are one of the most widely known shear instabilities. KH instabilities have been studied extensively in both homogeneous and stratified fluids using laboratory experiments (e.g., Refs. [1–3]), field observations [4–6], and numerical simulations (e.g., Refs. [7–14]). They are characterized by two-dimensional periodic elliptic vortices called KH billows, which are connected by thin tilted braids of high strain rate [15].

KH instabilities are susceptible to several secondary instabilities, e.g., vortex pairing [1,3,16,17], convective core instability due to the overturn of fluid caused by the roll-up (e.g., Refs. [7,8]), and instabilities that are located in braid regions and extract energy from the mean shear or strain (see Ref. [9]). Which secondary instabilities exist or dominate depends on nondimensional parameters governing the flows, i.e., Reynolds number, Richardson number, and Prandtl number. Klaassen and Peltier [18] verified that vortex pairing is the most unstable two-dimensional secondary instability. Strong stratification can inhibit vertical motion and suppress pairing [19]. Mashayek and Peltier [9,19] show that three-dimensional secondary instabilities grow faster in high Reynolds number flows and can destroy the two-dimensional coherent structure required for vortex pairing. The critical Reynolds number at which pairing does not occur decreases with increasing Richardson

 

TABLE I. Numerical parameters for all the simulations. The number of grid points is for the velocity field and is half that of the density field.

| Re | Pr | $J$ | $L_x/h_0$ | $L_y/h_0$ | $L_z/h_0$ | $N_x$ | $N_y$ | $N_z$ |
|---|---|---|---|---|---|---|---|---|
| 1200 | 16 | 0.07 | 14.43 | 7.22 | 15 | 320 | 160 | 320 |

number. Klaassen and Peltier [8], Mashayek and Peltier [9], and Salehipour and Peltier [13] have shown that high Prandtl number can increase the growth rate of some three-dimensional secondary instabilities, e.g., the secondary core instability.

However, in low to intermediate Reynolds number flows, which are applicable to some mixing layers [20] and environmental flows ([21], see Table 1), vortex pairing is the dominant two-dimensional secondary instability. The pairing instability results from a coincident subharmonic of the most unstable wave number that forces neighboring KH billows to combine (pair). It can increase the vertical scale of motion and thickness of the shear layer [22–24]. As a result, the effective Reynolds number is also increased. Since the amount of mixing and mixing efficiency are higher for higher Reynolds numbers in the mixing transition regime [12], vortex pairing can enhance mixing and mixing efficiency. The dominant three-dimensional secondary instability in this Reynolds number regime is the convective core instability [7,8]. Caulfield and Peltier [7] show that the growth rate of the convective core instability mainly comes from the mean shear, while the two-dimensional KH instability acts as a catalyst in the sense that it provides the flow on which the secondary instability grows. The competition of vortex pairing and three-dimensional secondary instabilities determines whether vortex pairing occurs or not. This competition is dependent on the initial nondimensional parameters, and also on the details of the initial perturbations [7,25], e.g., the amplitudes of KH, the subharmonic components, and three-dimensional motions.

Some researchers have studied the dependence of secondary instabilities on initial conditions in shear layers without density stratification [11,16,25–28]. Patnaik *et al.* [11] show that shredding replaces pairing when the phase relationship between KH and the subharmonic modes is unfavourable for pairing. One vortex is strengthened and the other is weakened in that case. However, shredding is seldom observed in experiments due to the existence of ambient noise other than pure eigenfunctions of the Orr-Sommerfeld equation. Ho and Huang [16] study the spreading rate of a spatially varied shear layer under different forcing. They show that without including the subharmonic mode in the initial perturbations pairing is significantly delayed. Metcalfe *et al.* [25] demonstrate that vortex pairing can suppress the modal growth rate of a three-dimensional mode when the subharmonic mode reaches finite amplitude and the three-dimensional mode is small. However, this may only be valid for flows initialized by eigenfunctions of sufficient amplitudes. Hajj *et al.* [26] show that the growth of the subharmonic mode is maximum close to an optimal phase difference between the KH and the subharmonic mode and is suppressed at other phase differences. Similarly, Husain and Hussain [28] demonstrate that at a phase difference unfavourable for pairing, and also for angles close to this phase difference, the growth rate of the subharmonic mode reduces significantly. The phase difference between different modes of the instability in the initial conditions has also been shown to influence the rate of mixing and flow structure in Rayleigh-Taylor instabilities [29].

Numerical investigations of shear instabilities in stratified flows have also found that vortex pairing depends on initial conditions, e.g., Klaassen and Peltier [18] and Smyth and Peltier [23]. Klaassen and Peltier [18] obtain the amplitude ratios of the first three harmonics with wave number $\frac{1}{2}\alpha_{kh}$, $\alpha_{kh}$, and $\frac{3}{2}\alpha_{kh}$, where $\alpha_{kh}$ is the wave number of the most unstable mode to the viscous Taylor-Goldstein (TG) equation [30,31], in a two-wavelength domain from a numerical simulation perturbed by white noise. They demonstrate that pairing is delayed and the growth rate of the subharmonic mode is decreased if the subharmonic and the third modes are out of phase relative to KH instabilities. In general, the time of vortex pairing may be sensitive to the phase of the $\frac{3}{2}\alpha_{kh}$

mode if the subharmonic mode is out of phase with KH mode. Smyth and Peltier [23] reached a similar conclusion about the effect of the phase on pairing.

Previous studies only considered the effect of initial conditions on pairing in two-dimensional simulations and mostly used eigenfunctions as initial perturbations. We extend these studies to examine the effects of phase difference between KH and subharmonic components in two- and three-dimensional flows with eigenfunction and random initial perturbations. Two-dimensional simulations are used to compare random perturbation simulations with eigenfunction perturbation simulations in terms of vortex pairing and sensitivity of pairing to the phase difference between the KH and subharmonic mode. Three-dimensional simulations are used to investigate the effect of three-dimensional motions on pairing and mixing.

The paper is organized as follows. The numerical methods and diagnostic tools are described in Sec. II. A simplified pairing mechanism is described in Sec. III. Section IV describes the process of vortex pairing using the Lagrangian trajectory, the phase shift and the growth rate of the subharmonic mode in two-dimensional simulations. In Sec. V, three-dimensional results are compared with two-dimensional results to study the effect of three-dimensional motions and mixing properties are compared in different simulations.

## II. METHODOLOGY

### A. Mathematical model

The unperturbed background flow is a pure horizontal stratified shear flow. The background velocity $\overline{U}$ and density $\overline{\rho}$ are hyperbolic tangent functions of vertical coordinate $z$, as first introduced by Hazel [32],

$$\bar{\rho} = -\frac{\Delta\rho}{2}\tanh\left(\frac{2z}{\delta_0}\right), \tag{1a}$$

$$\overline{U} = \frac{\Delta U}{2}\tanh\left(\frac{2z}{h_0}\right), \tag{1b}$$

where $\Delta U$ and $\Delta\rho$ are the variations of velocity and density respectively, $\delta_0$ is the thickness of the density interface, and $h_0$ is the thickness of the velocity interface. Four nondimensional parameters characterize the flows, i.e., the bulk Richardson number $J$, the Reynolds number Re, the Prandtl number Pr, and the scale ratio $R$ which are defined as

$$J = \frac{\Delta\rho g h_0}{\rho_0(\Delta U)^2}, \quad \mathrm{Re} = \frac{\Delta U h_0}{\nu}, \quad \mathrm{Pr} = \frac{\nu}{\kappa}, \quad R = \frac{h_0}{\delta_0}, \tag{2}$$

where $\kappa$ is molecular diffusivity, $\nu$ is kinetic viscosity, $\rho_0$ is a reference density. Here, we use the total velocity difference, density difference, and shear layer thickness to define the dimensionless parameters, while in some studies half of these scales are used (e.g., see Caulfield and Peltier [7]). In this study, $J = 0.07$, $\mathrm{Re} = 1200$, $\mathrm{Pr} = 16$, $R = 1$. The motivation for studying flows with $\mathrm{Pr} \gg 1$ is that for the diffusion of heat in water, Pr varies from 7.1 at 20°C to 13.4 at 0°C and for the diffusion of salt in water, Pr varies from 666 at 20°C to 1264 at 0°C [33]. Our choice of $\mathrm{Pr} = 16$ was influenced by these environmental values and computational restrictions. The flow is susceptible to Kelvin-Helmholtz instabilities for this combination of $J$ and $R$ (see Ref. [34], for a review of instability types).

We assume the fluid is incompressible and apply the Boussinessq approximation for small density difference, so the governing equations for the system are

$$\nabla \cdot \boldsymbol{u} = 0, \tag{3}$$

$$\frac{D\boldsymbol{u}}{Dt} = -\frac{1}{\rho_0}\nabla p - \frac{\rho}{\rho_0}g\hat{\boldsymbol{k}} + \nu\nabla^2\boldsymbol{u}, \tag{4}$$

$$\frac{D\rho}{Dt} = \kappa\nabla^2\rho, \tag{5}$$

where $u$ and $p$ are the fluid's velocity and pressure, respectively, and $\hat{\boldsymbol{k}}$ is the unit vertical vector. $D/Dt$ is the material derivative and $g$ is the gravitational acceleration.

### B. Direct numerical simulations

The governing Eqs. (3), (4), and (5) are solved by a pseudospectral code developed by Winters *et al.* [35] and later improved by Smyth *et al.* [36]. The code employs a third-order Adams-Bashforth time-stepping scheme. Boundary conditions are horizontally periodic and vertically free slip and no flux for our simulations.

The domain length $L_x$ is set to two wavelengths of the most unstable mode to allow vortex pairing. The spanwise width of the domain $L_y$ for the three-dimensional simulations is one wavelength of the primary KH instability, which is at least six wavelengths of the most unstable spanwise mode (for the most unstable spanwise wave number, see Ref. [18]). The domain height is $15h_0$, which is sufficient to remove the effects of the top and bottom boundaries on pairing [9,12]. The numerical details are summarized in Table I.

The resolution of DNS is typically determined by the Kolmogrov scale, $L_k = (\nu^3/\varepsilon')^{1/4}$, in homogeneous fluids where $\varepsilon'$ is the viscous dissipation rate of turbulent kinetic energy. Moin and Mahesh [37] suggest that the grid spacing in DNS should be $O(L_k)$. In stratified flows with $\mathrm{Pr} > 1$, the smallest scale that need to be resolved is $O(L_B)$, where $L_B$ is the Batchelor scale [38] and $L_B = L_k/\sqrt{\mathrm{Pr}}$. In our simulations, $\Delta z/L_B$ is always less than 4.0 and $\Delta z/L_K$ is always less than 2.0 (grid spacing of the density field is half of that of the velocity field). The dissipation rate $\varepsilon'$ used to calculate $L_K$ is averaged within $L_z/2 - h_0/2 < z < L_z/2 + h_0/2$, where turbulence is the most energetic. Although previous studies have used finer resolutions, e.g., Smyth and Winters [34] and Rahmani *et al.* [12], more recent studies, e.g., Salehipour and Peltier [13], have used similar resolutions. We also ran a resolution test for simulation $R\frac{\pi}{2}3D$ (Table II) with a double resolution. The final amount of mixing in the simulation with the finer resolution changed by less than 0.1%.

We ran two sets of simulations to study the effect of initial perturbations on vortex pairing and mixing. One set is perturbed by random perturbations, where three simulations are performed in both two and three dimensions. The energy of initial random perturbations projected on each two-dimensional Fourier component is almost the same. The other set is perturbed by the eigenfunctions to the TG equation of the KH and the subharmonic modes with the same amount of kinetic energy of the KH and the subharmonic mode [defined in Eq. (13)] as in random perturbation simulations. The eigenfunctions are obtained by solving TG equation using a second-order finite difference method. The eigenfunction simulations are performed in two dimensions only. The simulations are listed in Table II with key resultant times. In all the simulations in Table II, the initial amplitude ratio between the energy of the KH and the subharmonic components is one. In the Appendix, we examine the effects of the initial amplitude ratio for the simulation $E02D$.

For random perturbation simulations, random perturbations of $u'$ and $w'$ are added to the background flow. To simplify comparisons between 2D and 3D simulations, we used perturbations in $u'$ and $w'$ only. The perturbations quickly become fully three-dimensional in 3D simulations. The perturbations in $u'$ and $w'$ are given by the following equations:

$$u' = ar_u(x, y, z)\frac{\Delta U}{2}\left[1 - \left|\tanh\left(\frac{2z}{h_0}\right)\right|\right], \tag{6}$$

$$w' = ar_w(x, y, z)\frac{\Delta U}{2}\left[1 - \left|\tanh\left(\frac{2z}{h_0}\right)\right|\right], \tag{7}$$

where $r_u$ and $r_w$ are random numbers between $-1$ and 1, and $a$ sets the maximum amplitude of perturbations.

In the present study, $a = 0.1$, as in the simulations of Smyth and Winters [34] and Carpenter *et al.* [39], and small enough for perturbations to grow linearly initially. The initial conditions in

TABLE II. Definition of phase and important times and list of simulations. The simulations beginning with $E$ are perturbed by eigenfunctions, while those beginning with the letter $R$ are perturbed by random perturbations. The phase difference (0, $\pi/4$, or $\pi/2$) and the dimensions of each simulation appear in the name of the simulation. We also performed three-dimensional random perturbation simulations with phase differences $-0.125\pi$, $-0.375\pi$, and $-0.45\pi$ (not listed in the table) for mixing quantifications.

| | Random perturbations | | | | | | Eigenfunctions | |
|---|---|---|---|---|---|---|---|---|
| Run | $R02D$ | $R\frac{\pi}{4}2D$ | $R\frac{\pi}{2}2D$ | $R03D$ | $R\frac{\pi}{4}3D$ | $R\frac{\pi}{2}3D$ | $E02D$ | $E\frac{\pi}{2}2D$ |
| $\theta^M_{\rm sub}/\pi$ | 0.04 | −0.21 | −0.46 | 0.05 | −0.21 | −0.48 | 0 | 0.5 |
| $t_M$ | 24 | 24 | 24 | 24 | 24 | 24 | 0 | 0 |
| $t_{\rm kh}$ | 80 | 82 | 85 | 80 | 81 | 84 | 81 | 87 |
| $t_{\rm sub}$ | 106 | 110 | 146 | 107 | 113 | 129 | 104 | 249 |
| $t_p$ | 108 | 112 | 148 | 109 | 113 | – | 107 | 249 |
| $t_{3d}$ | – | – | – | 143 | 146 | 123 | – | – |
| $t_f$ | – | – | – | 231 | 221 | 186 | – | – |

| Parameter | Definition | Reference figure |
|---|---|---|
| $\theta^M_{\rm sub}$ | phase difference between the primary KH and subharmonic mode | Fig. 4(a) |
| $t_M$ | onset of modal growth, time when $r = 0.99$ | Fig. 3 |
| $t_{\rm kh}$ | first peak in kinetic energy of the primary KH | Fig. 6 |
| $t_{\rm sub}$ | global peak in the kinetic energy of the subharmonic | Fig. 6 |
| $t_p$ | when pairing vortices initially cross | Fig. 4(b) |
| $t_{3d}$ | first peak in the 3D kinetic energy | Fig. 6 |
| $t_f$ | first time $\mathrm{Re}_b < 20$ after a peak in 3D kinetic energy | |

two-dimensional simulations are spanwise averaged values of those in corresponding three-dimensional simulations.

We define the phase of each wave-number component in terms of two-dimensional vertical velocity $w_{2d}$ [defined in Eq. (9b)], i.e.,

$$\theta_k = \frac{\pi}{2} + \arg\left\{\hat{w}_{2d,k}\left(z = \frac{L_z}{2}\right)\right\}, \tag{8}$$

where arg is the argument or phase of a complex number, $\frac{\pi}{2}$ is added to make the vertical velocity $\Re\{\hat{w}_{2d,k}e^{i2k\pi x/L_x}\}$ of a specific mode a sine wave, and $\hat{w}_{2d,k}$ is the $k$th Fourier component of spanwise averaged vertical velocity $w_{2d}$. Klaassen and Peltier [18] and Smyth and Peltier [23] use a similar definition in terms of streamfunction. We use "component" to denote the Fourier component and "mode" to denote eigenfunction of a specific wave number throughout the paper. When a component becomes approximately modal after a nonmodal growth, we call it a mode. Note that $k = 2$ corresponds to the KH component and $k = 1$ corresponds to the subharmonic component, i.e., a wavelength equal to the domain length, $L_x$.

For random initial perturbations, initially each Fourier component experiences a nonmodal growth and the phase of every component defined in Eq. (8) changes. When the subharmonic component becomes approximately modal, i.e., identical to the eigenfunction of the TG equation (this occurs around nondimensional time $t\Delta U/h_0 = 24$ for the random perturbation simulations), the phase becomes almost constant for some time until nonlinear effects become important. We define $\theta_{\rm sub}$ as the phase of the subharmonic component relative to the KH component and $\theta^M_{\rm sub}$ as the value of $\theta_{\rm sub}$ when the subharmonic component becomes modal (defined in Sec. IV A). We examine the effects of the phase difference between the KH and subharmonic mode by considering three different phases in our random perturbation simulations. To determine the appropriate initial

phase difference, we first determine the phase shift that occurs in the premodal phase. We run a simulation with the random perturbation generated using Eqs. (6) and (7) until $t_M$ [e.g., $t = 24$ in Fig. 4(a)] and then calculate the phase shift of the subharmonic mode. Then we run the three simulations with the initial phase of the subharmonic set such that at $t = t_M$, $\theta^M_{\rm sub}$ is approximately 0, $-\pi/4$, and $-\pi/2$. These random simulations are designated by $R$ followed by the approximate modal phase $\theta^M_{\rm sub}$, and $2D$ or $3D$ depending on the number of dimensions of the simulation. For example, $\theta^M_{\rm sub}$ is approximately 0, $-\frac{\pi}{4}$, and $-\frac{\pi}{2}$, respectively, in three-dimensional simulations $R03D$, $R\frac{\pi}{4}3D$, and $R\frac{\pi}{2}3D$ (exact phase values are listed in Table II). It will be explained in Sec. IV E that the sign of the phase is not important.

Simulations perturbed by eigenfunctions are named by the same procedure, but the first letter is $E$, indicating that they are perturbed by eigenfunctions. For these eigenfunction perturbed simulations, the phase of the subharmonic mode does not change initially and $\theta^M_{\rm sub}$ is equal to the initial phase value. $\theta^M_{\rm sub} = -\frac{\pi}{2}$ for $E\frac{\pi}{2}2D$ and $\theta^M_{\rm sub} = 0$ for $E02D$.

### C. Diagnostic tools

Following Caulfield and Peltier [7], the velocity is decomposed into three parts, i.e.,

$$\overline{\boldsymbol{u}} = \langle \boldsymbol{u} \rangle_{xy}, \tag{9a}$$

$$\boldsymbol{u}_{2d} = \langle \boldsymbol{u} \rangle_{y} - \langle \boldsymbol{u} \rangle_{xy}, \tag{9b}$$

$$\boldsymbol{u}_{3d} = \boldsymbol{u} - \overline{\boldsymbol{u}} - \boldsymbol{u}_{2d}, \tag{9c}$$

where the subscripts indicate averaging over that direction. Given these definitions, the total kinetic energy $K$ is defined as

$$K = \frac{\langle \boldsymbol{u} \cdot \boldsymbol{u} \rangle_{xyz}}{2\rho_0 \Delta U^2}, \tag{10}$$

where $\rho_0 \Delta U^2$ is used for nondimensionalization, and can be partitioned into three parts $\overline{K}$, $K_{2d}$, $K_{3d}$, i.e.,

$$K = \overline{K} + K_{2d} + K_{3d}, \tag{11}$$

where

$$\overline{K} = \frac{\langle \overline{\boldsymbol{u}} \cdot \overline{\boldsymbol{u}} \rangle_{z}}{2\rho_0 \Delta U^2}, \tag{12a}$$

$$K_{2d} = \frac{\langle \boldsymbol{u}_{2d} \cdot \boldsymbol{u}_{2d} \rangle_{xz}}{2\rho_0 \Delta U^2}, \tag{12b}$$

$$K_{3d} = \frac{\langle \boldsymbol{u}_{3d} \cdot \boldsymbol{u}_{3d} \rangle_{xyz}}{2\rho_0 \Delta U^2}. \tag{12c}$$

Fourier transforms are applied to $u_{2d}$ and $w_{2d}$ to identify the contribution of each wave-number component $K_{2d}$, so that the kinetic energy of the $k$th component is

$$K_{2d,k} = \frac{\langle |\hat{u}_{2d,k}|^2 + |\hat{w}_{2d,k}|^2 \rangle_z}{\rho_0 \Delta U^2}, \quad k \geqslant 1, \tag{13}$$

where $\hat{u}_{2d,k}$ and $\hat{w}_{2d,k}$ are the Fourier components of $u_{2d}$ and $w_{2d}$ of wave number $2\pi k/L_x$. Hence,

$$K_{2d} = \sum_{k=1}^{\frac{N_x}{2}} K_{2d,k}. \tag{14}$$

Note that $k = 1$ corresponds to the subharmonic component and we denote it as $K_{\rm sub}$. $k = 2$ corresponds to the KH instability and we denote it as $K_{\rm kh}$.

We follow the framework in Winters *et al.* [40] to study mixing. The potential energy is then defined as

$$P = \frac{g\langle \rho z \rangle_{xyz}}{\rho_0 \Delta U^2}. \tag{15}$$

Potential energy $P$ is partitioned into background potential energy $P_b$ and available potential energy $P_a$ defined as

$$P_b = \frac{g\langle \rho z_b \rangle_{xyz}}{\rho_0 \Delta U^2}, \quad P_a = P - P_b, \tag{16}$$

where $z_b$ is the location of fluid parcels after being rearranged into a statically stable state (see Ref. [40]). Available potential energy characterizes the energy that can be exchanged between potential energy and kinetic energy, while the increase in background potential energy quantifies irreversible mixing in a closed system. The amount of mixing caused by the fluid's motion is

$$M = \Delta P_b - D \equiv \int \phi_M dt, \tag{17}$$

where $\phi_M$ is defined as the rate of mixing and $D$ is the mixing caused by molecular diffusion in quiescent fluid and calculated by

$$D = \frac{-\kappa g(\bar{\rho}|_{z=L_z} - \bar{\rho}|_{z=0})t}{L_z} \frac{1}{\rho_0 \Delta U^2}. \tag{18}$$

During the whole process, $D$ grows approximately linearly. The instantaneous mixing $\phi_M$ is always positive and varies over time. Cumulative mixing efficiency [7] is used as a measure of overall mixing properties in this study. It is defined as

$$E_c^{t_{3d}-t_f} = \frac{\int_{t_{3d}}^{t_f} \phi_M dt}{\int_{t_{3d}}^{t_f} \phi_M dt + \int_{t_{3d}}^{t_f} \varepsilon dt}, \tag{19}$$

where $t_{3d}$ is the time when $K_{3d}$ reaches its maximum and $t_f$ is defined as the time when buoyancy Reynolds number $\mathrm{Re}_b = \varepsilon'/\nu\langle N^2 \rangle_z$ first drops below 20 after $t_{3d}$. To compute $\mathrm{Re}_b$, we average $N^2$ and $\varepsilon'$ over an active range of turbulence where density gradients are significant, as proposed by Smyth and Moum [41]. The computed mixing efficiency showed a small sensitivity to the choice of $t_f$ as long as $t_f$ represented a time in the relaminarization stage. This period is chosen as previous investigations show that turbulence is active only when $\mathrm{Re}_b > 20$ [41]. By choosing $t > t_{3d}$, we remove the two-dimensional mixing because mixing caused by two-dimensional overturns is process dependent [42–44] and specifically depends on initial perturbation. To examine the effects of pairing on the mixing efficiency of a complete mixing event, we also consider a cumulative mixing efficiency, $E_c^{t_0-t_f}$, where the mixing efficiency in Eq. (19) is computed between $t = 0$ and $t_f$. Hereafter, time is nondimensionalized by $h_0/\Delta U$ and we refer to $t$ as the dimensionless time.

## III. PAIRING MECHANISM

The pairing process and the importance of the phase of the subharmonic are illustrated in Fig. 1. In Fig. 1(a), the subharmonic mode displaces the left KH billow upward and the right KH billow downward. The two KH billows are then advected toward each other by the mean flow, cross each other, and merge into one larger billow. This is the optimal phase for pairing. In Fig. 1(b), the phase of the subharmonic mode is $\theta_{\mathrm{sub}} = -\frac{\pi}{2}$ and two KH core centers are at the nodes of the subharmonic mode. This is called the "shredding mode" in Patnaik *et al.* [11] and the "draining mode" in the discussions by Klaassen and Peltier [18] and Smyth and Peltier [23]. In this case, one KH vortex

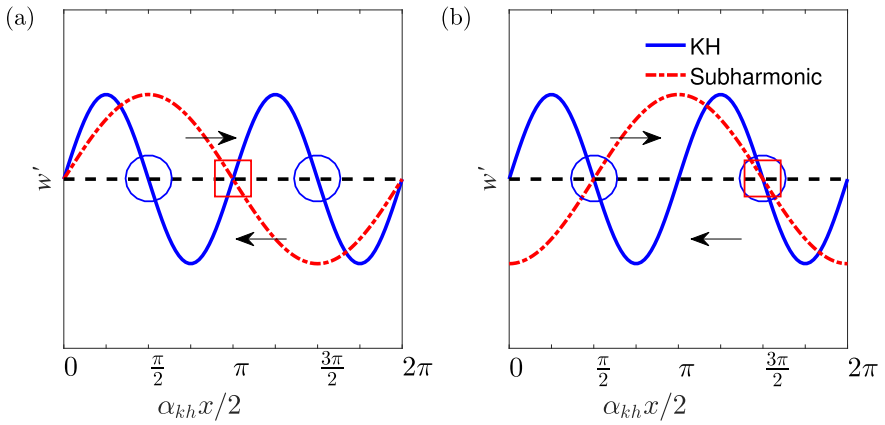


FIG. 1. Conceptual drawing of vortex pairing demonstrating the effect of phase of the subharmonic mode. (a) $\theta_{\text{sub}} = 0$, (b) $\theta_{\text{sub}} = -\frac{\pi}{2}$. The blue solid line is KH mode and the red dash-dotted line is the subharmonic mode. Blue circles denote the location of KH vortex centers and red squares are vortex centers associated with the subharmonic mode. The two arrows show the directions of the mean flow.

[the right one in Fig. 1(b)] is strengthened by the subharmonic mode and the other KH vortex [the left one in Fig. 1(b)] is weakened by the straining field of the subharmonic mode. For example, in Fig. 1(b), the right vortex will be stronger than the left one.

Resultant KH billows with and without pairing are illustrated in the vorticity snapshots from DNS in Fig. 2. At $t = 106$, the simulation with the phase of subharmonic mode $\theta_{\text{sub}} = 0$, $R02D$, is undergoing a vortex merging, while the simulation with $\theta_{\text{sub}} = -\frac{\pi}{2}$, $\theta_{\text{sub}} = 0$, $R\frac{\pi}{2}2D$, exhibits a draining mode. In $R\frac{\pi}{2}2D$, the pairing mode eventually grows and surpasses the KH mode. During this adjustment, the phase of the subharmonic mode shifts toward 0. We discuss this pairing process in Sec. IV. In three-dimensional simulations, the growth of three-dimensional motions disintegrates the two-dimensional structure of the billows and can inhibit the merging of the billows; see simulations $R03D$ and $R\frac{\pi}{2}3D$ at $t = 146$. We discuss these effects in Sec. V.

## IV. TWO-DIMENSIONAL ASPECTS OF PAIRING

In this section, we examine the 2D pairing process focusing on comparing pairing in flows perturbed by eigenfunctions with flows perturbed by random perturbations. Besides the traditional phase and growth rate analysis, we characterize the degree of modality quantitatively and use Lagrangian trajectories to aid in the interpretation of the Fourier decomposition.

### A. Degree of modality

We use the cosine of Hermitian angle [45] between the subharmonic component $\hat{w}_{2d,\text{sub}}$ and the initial eigenfunction of the subharmonic mode $\hat{w}_{\text{eig,sub}}$ to quantify the degree of modality,

$$r(t) = \frac{|(\hat{w}_{2d,\text{sub}}, \hat{w}_{\text{eig,sub}})|}{|\hat{w}_{2d,\text{sub}}||\hat{w}_{\text{eig,sub}}|}, \tag{20}$$

where $(\cdot, \cdot)$ denotes the standard scalar product for complex vectors and $||$ denotes the amplitude of a complex number. $r(t)$ is the ratio between the length of the orthogonal projection of the subharmonic component onto the the eigenfunction to the length of itself. It is always between 0 and 1, and equal to 1 only when the subharmonic component of the random perturbation is identical to the eigenfunction.

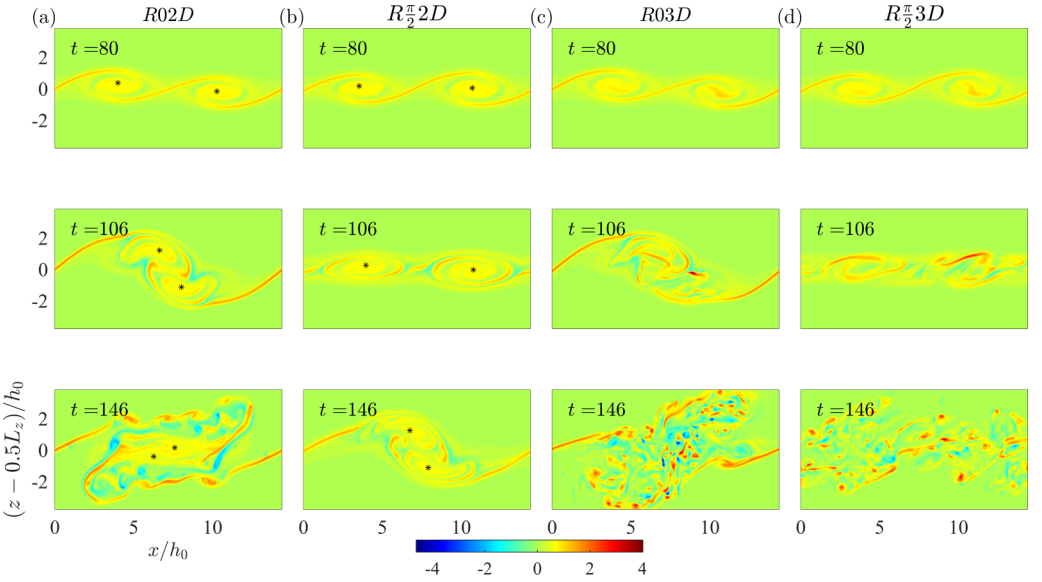


FIG. 2. Nondimensional spanwise vorticity $(u_z - w_x)h_0/\Delta U$ of two-dimensional simulations $R02D$ (phase of the subharmonic mode is $\theta^M_{\text{sub}} \approx 0$) and $R\frac{\pi}{2}2D$ (phase of the subharmonic mode is $\theta^M_{\text{sub}} \approx -\frac{\pi}{2}$) and their corresponding three-dimensional simulations $R03D$ and $R\frac{\pi}{2}3D$. The snapshots of three-dimensional simulations are plotted at $y = \frac{L_y}{2}$. Pairing is delayed in two-dimensional simulation $R\frac{\pi}{2}2D$ but completely eliminated in the three-dimensional simulation $R\frac{\pi}{2}3D$. Black stars are fluid particles located at vortex centres at $t = 30$.

Figure 3 shows the evolution of $r$ for the three random perturbation simulations $R02D$, $R\frac{\pi}{4}2D$, and $R\frac{\pi}{2}2D$. Initially, $r$ is small because the subharmonic component of the initial random perturbations is significantly different from the eigenfunction. As the subharmonic component evolves to the eigenfunction, $r$ increases to 1. We define the time required for the subharmonic component to become modal, $t_M$, as the time when $r$ first exceeds 0.99, which is $t = 24$ for these three simulations.

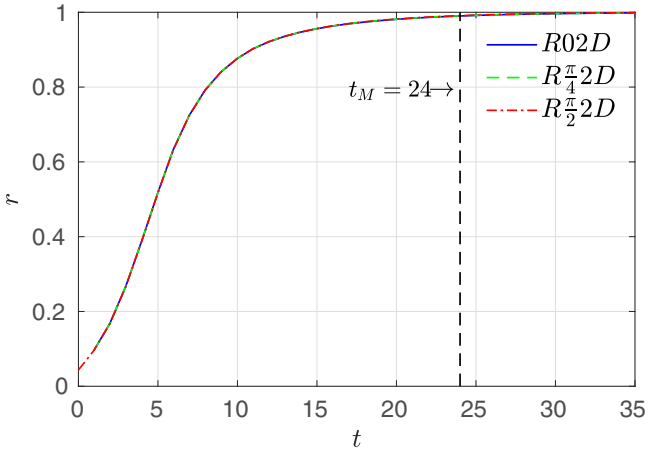


FIG. 3. Evolution of $r$ for random perturbation simulations $R02D$, $R\frac{\pi}{4}2D$, and $R\frac{\pi}{2}2D$.

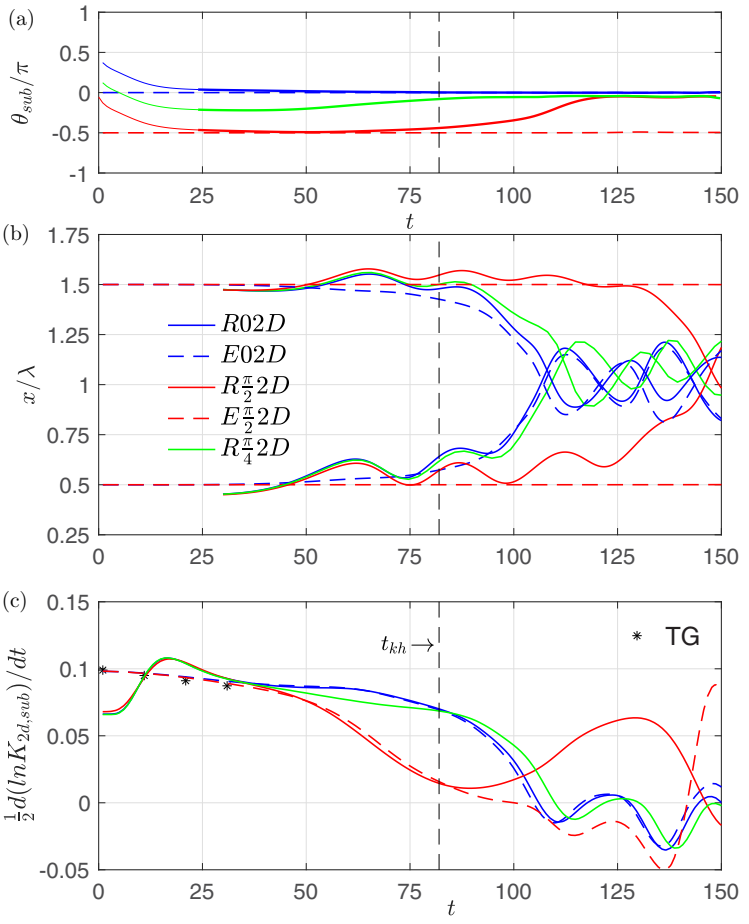


FIG. 4. (a) Evolution of the phase of the subharmonic component. The phase before $t_M$ is shown as thin lines. The phase shift in simulation $E\frac{\pi}{2}2D$ begins after $t = 150$ and is not shown in this figure. (b) $x$ coordinates of two fluid particles located at the two vortex centers at $t = 30$ for random perturbation simulations and at $L_x/4$ and $3L_x/4$ for eigenfunction perturbation simulations. Pairing occurs at $t = 249$ for simulation $E\frac{\pi}{2}2D$ and is not shown in this figure. (c) Growth rate of the subharmonic mode. The vertical dashed line indicates the saturation time of KH instabilities in simulation $R\frac{\pi}{4}2D$. The stars labeled as TG indicate the growth rate calculated using the TG equation with the time-dependent mean flow.

Before $t = 24$, the three simulations appear identical in Fig. 3 because the subharmonic component is evolving linearly, i.e., nonlinear interaction of different components is negligible.

### B. Phase evolution

The phases for the five two-dimensional simulations perturbed by random perturbations and the eigenfunctions are plotted in Fig. 4(a). Initially, in the eigenfunction perturbation simulations, the phase does not change. In the three random perturbation simulations, before $t = 24$, the phases change because of nonmodal growth. The premodal phase (before $t_M$) in the random perturbation simulations is therefore shown as a thin line. Between $t = 24$ and $t = 50$, the phases stay almost constant. During this period, the phases are approximately $0, -\frac{\pi}{4}, -\frac{\pi}{2}$ for $R02D$, $R\frac{\pi}{4}2D$, and $R\frac{\pi}{2}2D$, respectively (see Table II). After $t = 50$, the phases of the subharmonic mode in simulations $R\frac{\pi}{4}2D$ and $R\frac{\pi}{2}2D$ shift toward 0, which is similar to the results of Klaassen and Peltier [18]. For the

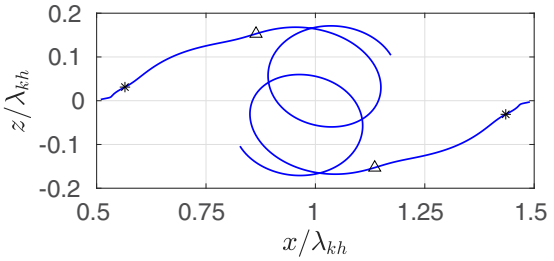


FIG. 5. The trajectories of two fluid particles between $t = 45$ and $t = 135$. The stars indicate $t_{\rm kh}$ and the triangles indicate $t_{\rm sub}$.

eigenfunction simulation $E\frac{\pi}{2}2D$, the phase begins to shift after $t = 200$ and is not shown in the figure. We ran a supplementary simulation perturbed by the KH, the subharmonic, and a third mode of wave number $\frac{3}{2}\alpha_{\rm kh}$, and found that the time of pairing is greatly reduced compared to the $E\frac{\pi}{2}2D$ simulation. This result is consistent with the earlier phase shift found in the three-mode simulations of Klaassen and Peltier [18].

### C. Trajectories of pairing KH billows

To characterize the trajectories of KH billows during pairing, fluid particles are introduced at a prescribed time at the KH vortex centers. The vortex centers are identified by the two inflection points of the contour $\rho = \rho_0$. In the randomly perturbed simulations the vortex centres are identified at $t = 30$, the earliest time when the KH vortices are clearly identifiable. In the case of the eigenfunction simulations the vortex centres are initially at $\frac{L_x}{4}$ and $\frac{3L_x}{4}$.

Figure 2 shows the evolution of the vorticity field with the two fluid particles shown as black stars. As the figure shows, these two fluid particles approximately represent the vortex centres until small-scale motions prevail, e.g., at $t = 146$ for simulation $R02D$. As an example, Fig. 5 shows the trajectories in the eigenfunction perturbation simulation $E02D$ with the optimal phase. The trajectories of the two particles are well organized and symmetric about the domain center because of the symmetry of the initial conditions. From $t_{\rm kh}$, defined as the time when $K_{\rm kh}$ reaches its first maximum (the global maximum is caused by vortex pairing), to $t_{\rm sub}$, defined as the time when $K_{\rm sub}$ reaches its global maximum, the KH billows undergo most of their vertical displacement. After this time, the billows cross over each other merging into the subharmonic billow, while the two vortex centres rotate around the domain center. The KH billow originally at the crest of the subharmonic remains, on average, elevated above the KH billow originally at the trough of the subharmonic. As will be shown in Sec. V, during this first orbit ($t = 107$ to $t = 119$) three-dimensional motions become important.

Now we return to Fig. 4(b), which shows the temporal variability of the horizontal coordinates of the two fluid particles. After approximately $t = 75$, the two fluid particles quickly converge in $x$ for the two optimal phase simulations $E02D$ and $R02D$. We defined the time of pairing, $t_p$, as the time when the horizontal distance first becomes zero and listed in Table II (for three-dimensional simulations, $t_p$ is obtained by averaging two sets of trajectories each composed of 21 fluid particles spread over the spanwise direction). The two vortices become closer and merge in simulation $E\frac{\pi}{2}2D$ at $t = 249$ (not shown in the figure). Unlike the results of the eigenfunction simulations, in the random perturbation simulations there is an oscillation of the fluid particles before $t_{\rm sub}$ and $t_p$ because of the existence of modes other than the KH and subharmonic modes. For these three random perturbation simulations, the horizontal distance between the two fluid particles is always the smallest for $R02D$ and largest for $R\frac{\pi}{2}2D$. Also, pairing occurs first in $R02D$ and last in $R\frac{\pi}{2}2D$, so $t_p^{R02D} < t_p^{R\frac{\pi}{4}2D} < t_p^{R\frac{\pi}{2}2D}$. Relating Fig. 4(b) with the phase evolution in Fig. 4(a), we find that the two fluid particles begin to move together (i.e., pair) only once the phase is approximately optimal. The

pairing therefore occurs earliest if the subharmonic is in phase and latest if it is out of phase similar to the previous studies of Klaassen and Peltier [18], Smyth and Peltier [23], Hajj *et al.* [26], and Husain and Hussain [28]. Comparison between $t_p^{R\frac{\pi}{4}2D}$ and $t_p^{R02D}$ indicates that if the subharmonic mode is not close to $\pm\frac{\pi}{2}$, the difference in pairing is small, as also observed by Husain and Hussain [28]. Also, the time of pairing for simulation $R02D$ is close to $E02D$, but the time of pairing for simulation $R\frac{\pi}{2}2D$ is much earlier than in simulation $E\frac{\pi}{2}2D$.

### D. Growth rate

Figure 4(c) shows the growth rate of the subharmonic component for the three random perturbation simulations and the two eigenfunction simulations. Initially, the growth rates of the subharmonic mode for the two eigenfunction simulations ($E02D$ and $E\frac{\pi}{2}2D$) are the same and decline as the shear layer diffuses. The estimated growth rate (labeled with TG) using the TG equation and the varying mean flow has the same decreasing trend as the growth rates based on $K_{\text{sub}}$. For the random perturbation simulations ($R02D$, $R\frac{\pi}{4}2D$, and $R\frac{\pi}{2}2D$), the growth rate during the nonmodal stage of growth can be either smaller or larger than the modal growth rate as found by Guha and Lawrence [46]. For all five simulations, the growth rate is independent of the phase in the initial linear stage of growth, i.e., before around $t = 45$.

After $t = 45$, nonlinear effects and the phase become important. After $t = 45$ and before $t_{\text{kh}}$, the growth rates in the late pairing simulations ($E\frac{\pi}{2}2D$ and $R\frac{\pi}{2}2D$) drop compared to the other simulations, in agreement with Klaassen and Peltier [18]. However, we find that the growth rate in the $R\frac{\pi}{4}2D$ simulation stays closer to the optimal phase simulations $R02D$ and $E02D$. The growth rates in simulations $R02D$ and $E02D$ are almost the same and the growth rates in simulations $R\frac{\pi}{2}2D$ and $E\frac{\pi}{2}2D$ are almost the same. This suggests that if the phase and amplitude of the subharmonic and KH are the same for an eigenfunction perturbation and a random perturbation, the growth rate of the subharmonic mode is the same before saturation of KH instabilities. In other words, the existence of the other components in initial perturbations and initial nonmodal growth have negligible effects on the growth rate during this nonlinear growth stage.

When the KH instability reaches its maximum amplitude ($t_{\text{kh}}$) the phase is close to optimal in $R02D$, $R\frac{\pi}{4}2D$, and $E02D$. The growth rates then quickly decrease to zero. In these three simulations, the first zero crossing of the growth rate is close to $t_p$ and denotes the saturation of the subharmonic mode, i.e., the global maximum of $K_{\text{sub}}$. In $R\frac{\pi}{2}2D$, after $t_{\text{kh}}$ the growth rate begins to increase along with the phase shifting toward the optimal value [see Fig. 4(a)]. In this simulation, the saturation of the subharmonic mode occurs at $t = 146$. In $E\frac{\pi}{2}2D$, the phase remains at $-\frac{\pi}{2}$ and the growth rate continues to decrease. Unlike the other simulations, the growth rate crosses zero before saturation of the subharmonic mode (at $t = 249$). Comparison between simulations $R\frac{\pi}{2}2D$ and $E\frac{\pi}{2}2D$ shows that the growth rate is sensitive to the initial structure of the subharmonic component or the existence of the other components in initial conditions if the phase is close to $-\frac{\pi}{2}$.

In Table II, the saturation times of KH and the subharmonic mode and time of pairing ($t_{\text{kh}}$, $t_{\text{sub}}$, and $t_p$) are summarized. Pairing occurs first in simulation $E02D$, second in $R02D$, third in $R\frac{\pi}{4}2D$, fourth in $R\frac{\pi}{2}2D$, and last in $E\frac{\pi}{2}2D$. In all simulations $t_{\text{sub}}$ is close to $t_p$, i.e., the global maximum in the kinetic energy of the subharmonic approximately coincides with the initial crossing of pairing KH billows. Ho and Huang [16] obtain a qualitatively similar result in the laboratory.

### E. Sensitivity of the time of pairing to the phase

We find that vortex pairing is sensitive to initial conditions when the phase of the subharmonic mode is close to $\pm\frac{\pi}{2}$. For simplicity in this discussion, we use $t_{\text{sub}}$ to characterize the time of pairing. Provided pairing occurs, this is generally accurate (i.e., $t_{\text{sub}} \sim t_p$). In general, $t_{\text{sub}}$ is a function of all modes in the initial conditions, not only the subharmonic mode.

We consider the sensitivity of $t_{\text{sub}}$ to the phase of the subharmonic mode by running two-dimensional simulations perturbed by KH and the subharmonic mode eigenfunctions. Since the

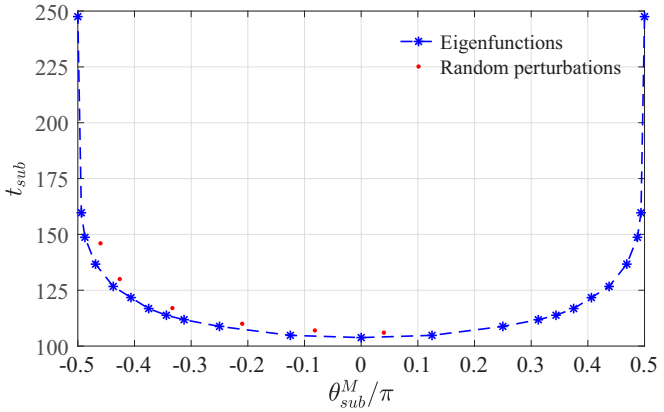


FIG. 6. Saturation time of the subharmonic mode, $t_{\text{sub}}$, as a function of the phase $\theta^M_{\text{sub}}$ for two-dimensional simulations perturbed by eigenfunctions and random perturbations. Note $t_{\text{sub}}$ is approximately equal to the time of pairing (see Table II).

initial velocity and density fields of phase $\theta^M_{\text{sub}}$ are the negatives of the reflection of velocity and density fields of phase $\theta^M_{\text{sub}}$ about the center of the domain and the governing equations conserve this symmetry, $t_{\text{sub}}$ is an even function of $\theta^M_{\text{sub}}$. Therefore, we only consider phases from $-\frac{\pi}{2}$ to 0 for random perturbations. We calculate $t_{\text{sub}}$ for 12 discrete phases between $-\frac{\pi}{2}$ and 0 and plot the results and the symmetric reflection between 0 and $\frac{\pi}{2}$ in Fig. 6. The figure shows that the time of pairing is not sensitive to the phase when the phase is close to 0. However, the time of pairing increases significantly near $\theta^M_{\text{sub}} = \pm\frac{\pi}{2}$, which indicates that $t_{\text{sub}}$ is sensitive to the phase when the phase is close to $\pm\frac{\pi}{2}$. Additional simulations (not shown) indicate that slight deviation from the eigenfunction of the subharmonic mode in initial conditions can also change the time of pairing. Hence, the delay of vortex pairing is sensitive to the functional form of the subharmonic component, phase, and other modes in two-dimensional simulations when the phase is close to $\pm\frac{\pi}{2}$. Detailed investigations of these effects are the subject of future studies.

Figure 6 also shows the time of pairing $t_{\text{sub}}$ for two-dimensional random perturbation simulations. The results show the same trend as the eigenfunction simulations, i.e., $t_{\text{sub}}$ increases with the phase. The initial nonmodal growth and existence of other modes in the initial conditions cause the slight difference between random perturbation and eigenfunction results. However, the significant increase of $t_{\text{sub}}$ near $\pm\frac{\pi}{2}$ can only occur in pure eigenfunction simulations since any deviation from the pure eigenfunctions in initial conditions will project on the pairing mode with phase 0 and reduce the time of pairing compared to pure eigenfunctions with phase $\pm\frac{\pi}{2}$.

The time of pairing can also be sensitive to the initial amplitude ratio between the KH and the subharmonic components. We examine this effect in the Appendix for the simulation $E02D$. The results in this Appendix suggest that while the time of pairing is sensitive to the initial amplitude ratio, the phase effects on the time of pairing are more significant. However, a more detailed study is required to understand the combined effects of phase and amplitude ratio. For the rest of the paper, we only consider cases where the KH and subharmonic components initially have the same level of energy.

## V. THREE-DIMENSIONALIZATION AND MIXING

### A. Three-dimensionalization

The growth of three-dimensional instabilities inhibits pairing. In simulation $R\frac{\pi}{2}3D$, where pairing is delayed, three-dimensional instabilities break down the two individual KH billows before pairing can occur, see Fig. 2, $t = 146$. In simulation $R03D$ pairing occurs before the growth of

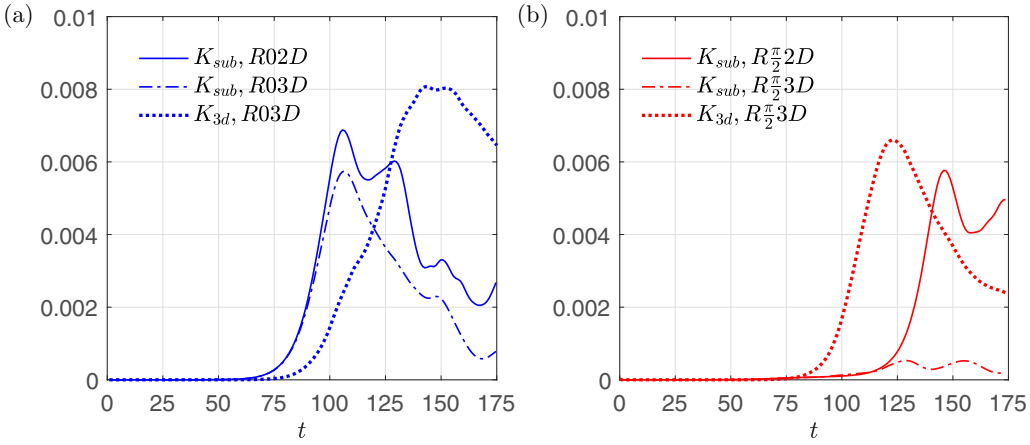


FIG. 7. Kinetic energy of the subharmonic mode $K_{\text{sub}}$ and three-dimensional kinetic energy $K_{3d}$ in two-dimensional and three-dimensional simulations: (a) $\theta^M_{\text{sub}} \approx 0$, (b) $\theta^M_{\text{sub}} \approx -\frac{\pi}{2}$.

three-dimensional instabilities and by $t = 146$ the two vortices have merged into the subharmonic billow; see Fig. 2.

To quantify the effects of three-dimensional motions on pairing, we compare the kinetic energy of the subharmonic component in two- and three-dimensional random perturbation simulations to the kinetic energy of three-dimensional motions (Fig. 7) for most and least favourable phase conditions for vortex pairing. Before the emergence of pairing (for $t < 75$), the total kinetic energy, $K_{2d}$ (not shown in the figure), is the same for all simulations as the growth of KH is similar in all cases. In the optimal phase simulation, i.e., $\theta^M_{\text{sub}} \approx 0$, the peak of the kinetic energy of the subharmonic mode, $K_{\text{sub}}$, is reduced slightly in the three-dimensional simulation, while the saturation time of the subharmonic mode is almost identical in the $2D$ and $3D$ simulations (see $R02D$ and $R03D$ in Fig. 7(a) and Table II). The peak in $K_{3d}$ occurs at $t = 143$, well after the peak in $K_{\text{sub}}$. These indicate that in cases with the phase at or near optimal the growth of three-dimensional motions has little effect on pairing.

For $\theta^M_{\text{sub}} \approx -\frac{\pi}{2}$, the peak of the kinetic energy of the subharmonic mode $K_{\text{sub}}$ is significantly lower in the three-dimensional simulation compared to the two-dimensional simulation [see Fig. 7(b)]. In the $R\frac{\pi}{2}3D$ simulation, the peak in $K_{3d}$ occurs earlier, at $t = 123$, and precedes the peak of $K_{\text{sub}}$ in both two- and three-dimensional simulations. During the extra time needed in $R\frac{\pi}{2}3D$ for the phase to shift from $-\frac{\pi}{2}$ to $\sim 0$, the three-dimensional motions grow and and destroy the two-dimensional coherent KH billows before vortex pairing occurs. Therefore, pairing is eliminated in simulation $R\frac{\pi}{2}3D$. The peak in $K_{3d}$ in simulation $R\frac{\pi}{2}3D$ is smaller compared to that in simulation $R03D$. The vortex pairing in simulation $R03D$ effectively increases the Reynolds number and makes the flow more energetic.

### B. Mixing

Figure 8(a) shows the increase in the total potential energy caused by the fluid's motion, $\Delta P - D$, with time. Time variation of $\Delta P - D$ is the same for the three simulations before $t = 80$. The first peak in $R03D$ and $R\frac{\pi}{4}3D$ represents vortex pairing and the first peak in $R\frac{\pi}{2}3D$ represents saturation of KH. The peak due to vortex pairing does not exist for $R\frac{\pi}{2}3D$ as pairing never occurs. Contrary to the results of Mashayek and Peltier [10], where vortex pairing occurred during the turbulent stage, the peak of $\Delta P - D$ due to vortex pairing occurs during the preturbulent stage due to our relatively low Reynolds number. Overall, the increase in total potential energy in cases with vortex pairing is much higher than the case without vortex pairing because vortex pairing efficiently increases the

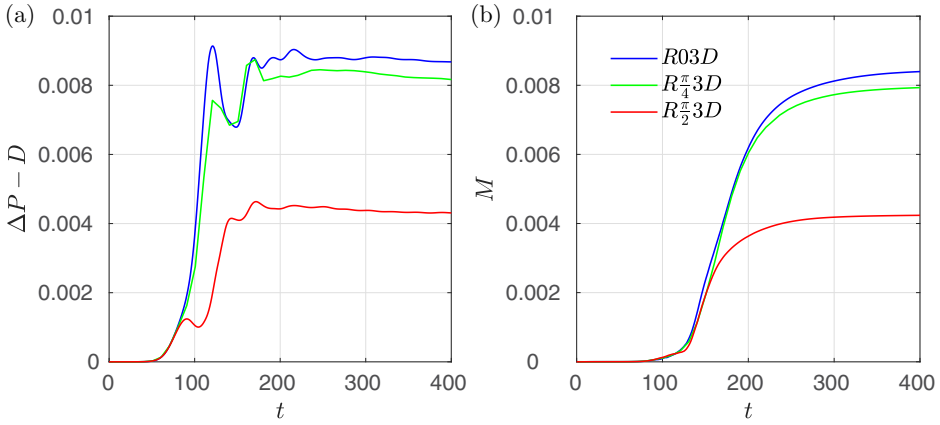


FIG. 8. (a) The increase in total potential energy caused by fluid's motion $\Delta P - D$, (b) the increase in mixing $M$.

vertical scale of fluid's motion and stirs the fluid. The increase in total potential energy in $R\frac{\pi}{4}3D$ is also slightly lower than in $R03D$.

Figure 8(b) shows the amount of mixing $M$. For all simulations, the amount of mixing is negligible before saturation of KH instabilities because the flow is still well-organized and mixing is mainly caused by laminar molecular diffusion. This is consistent with findings of Mashayek and Peltier [10], Rahmani *et al.* [47], and Salehipour and Peltier [13], which have shown that mixing is negligible before the KH billow reaches its maximum amplitude. After about $t = 130$, the amount of mixing significantly increases as small-scale motions reach sufficient amplitude and mixing occurs through turbulent diffusion. As turbulence subsides, the amount of mixing gradually approaches a constant. The final amount of mixing in simulation $R03D$ with vortex pairing is significantly higher than simulation $R\frac{\pi}{2}3D$ without pairing. The amount of mixing $M$ at $t = 400$ in simulation $R03D$ is double that of simulation $R\frac{\pi}{2}3D$. Mixing in simulation $R\frac{\pi}{4}3D$ is only slightly lower than that in simulation $R03D$.

We examine the dependence of the final amount of mixing $M$ and the cumulative mixing efficiency $E_c^{t_{3d}-t_f}$, defined in Eq. (19) as a measure of mixing efficiency during the active turbulence stage, on $\theta_{\text{sub}}^M$ in Fig. 9. In the same figure we also show the variation of the overall cumulative mixing efficiency, $E_c^{t_0-t_f}$, with $\theta_{\text{sub}}^M$. As the phase of the subharmonic mode relative to KH decreases from 0 to $-\frac{\pi}{2}$, mixing drops monotonically to less than half of its maximum value at $\theta_{\text{sub}}^M = 0$. However, this effect is less pronounced when the phase difference is close to optimal and mixing starts to sharply drop for $\theta_{\text{sub}}^M \leqslant -0.375\pi$. This is consistent with the laboratory experiments of Husain and Hussain [28] and Hajj *et al.* [26], where they observed the vortex pairing was suppressed over a range of phases close to the nonoptimal phase.

The turbulent phase cumulative mixing efficiency drops monotonically from 0.229 at $\theta_{\text{sub}}^M = 0$ to 0.198 at $\theta_{\text{sub}}^M = -\frac{\pi}{2}$, marking a 14% drop. The overall cumulative mixing efficiency drops 20%, from 0.193 to 0.155 as $\theta_{\text{sub}}^M$ varies from the optimal phase of 0 to the nonoptimal phase of $-\pi/2$. Therefore, the effect of phase on cumulative mixing efficiency is less pronounced compared to its effect on the amount of mixing. The effect of phase is more significant for the overall cumulative mixing efficiency, $E_c^{t_0-t_f}$, compared to the turbulent phase cumulative mixing efficiency, $E_c^{t_{3d}-t_f}$. The reason is the effects of the initial perturbations are more important during the initial laminar phases of the flow that are included in the overall cumulative mixing efficiency measurement. The overall mixing efficiency, $E_c^{t_0-t_f}$, is lower than the turbulent mixing efficiency, $E_c^{t_{3d}-t_f}$, contrary to the results of some previous studies [10,42,43] that found a highly efficient preturbulent mixing. This difference is because our Prandtl number is higher compared to these studies and so the preturbulent

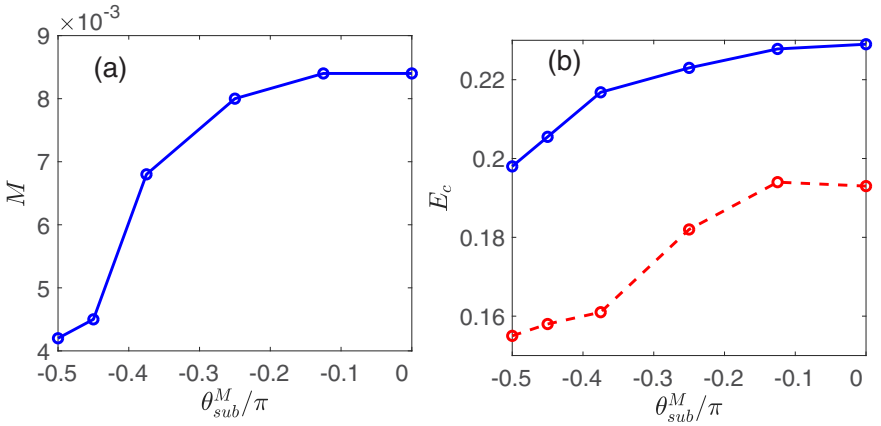


FIG. 9. The dependence of (a) the final amount of mixing $M$ and (b) the cumulative mixing efficiency $E_c$ on the phase difference between the primary KH and the subharmonic component, $\theta^M_{\rm sub}$. In panel (b) the solid line shows $E_c^{t_{3d}-t_f}$, the cumulative mixing efficiency computed from $t_{3d}$ to $t_f$, and the dashed line delineates the overall cumulative mixing efficiency, $E_c^{t_0-t_f}$, the cumulative mixing efficiency computed from $t=0$ to $t_f$.

mixing is small in our simulations (e.g., see Rahmani *et al.* [47]). Our random perturbations also induce a higher viscous dissipation in the beginning of the simulation and slightly lower mixing efficiency in the preturbulent stage. The range of $E_c^{t_{3d}-t_f}$ obtained here is close to the cumulative mixing efficiency of 0.2 commonly computed in other numerical studies [12,44,47–49], while the range of $E_c^{t_0-t_f}$ is slightly lower than 0.2. However, these studies have revealed some sensitivity of the mixing efficiency to the Reynolds number, Prandtl number, and the bulk Richardson number that can make direct comparisons to our results less straightforward.

## VI. CONCLUSIONS

We have investigated the effect of phase of subharmonic mode on vortex pairing and mixing using two-dimensional and three-dimensional DNSs. In two-dimensional simulations, we use a ratio to measure the extent to which that the subharmonic component deviates from the eigenfunction to the TG equation with the same wave number. That the ratio quickly increases to 1 from a small number shows that the nonmodal subharmonic component quickly evolves to the eigenfunction. We also track the Lagrangian trajectories of two fluid particles located at the centres of the KH vortices and their trajectories are shown to represent the vortex centres before small scale motions prevail. Similar to Ho and Huang [16], when kinetic energy of the subharmonic mode reaches its maximum, one KH vortex is almost on top of the other, i.e., $t_{\rm sub}$ coincides with $t_p$.

As Klaassen and Peltier [18] and Smyth and Peltier [23] have shown, if the subharmonic mode is out of phase, then it adjusts its phase and pairing is delayed. We have found that if the initial phase of the subharmonic mode is not close to $\pm\frac{\pi}{2}$, pairing is only slightly delayed and the flow perturbed by eigenfunctions behaves similarly to the flow perturbed by random perturbations. Before the KH instability reaches its first maximum in kinetic energy, i.e., before $t_{\rm kh}$, the growth rate of the subharmonic component is almost the same for the eigenfunction simulation and random perturbation simulation if the phase of the subharmonic component is the same. Moreover, the growth rate in the case where the phase is about $\frac{\pi}{4}$ is close to the case where the phase is 0. After $t_{\rm kh}$, if the phase is not close to $\pm\frac{\pi}{2}$, then the growth rate is still not sensitive to the initial perturbations. If the phase is close to $\pm\frac{\pi}{2}$, then the growth rate in the random perturbation differs significantly from that in the eigenfunction simulation and the subharmonic component reaches its maximum earlier in the random perturbation simulation. To investigate the sensitivity of time of pairing to the phase,

we ran simulations perturbed by the KH and subharmonic eigenfunctions with different phases. It is shown that $t_{\rm sub}$ increases with the phase of the subharmonic mode and it increases significantly at $\theta^M_{\rm sub} = \pm\frac{\pi}{2}$. Time of pairing and $t_{\rm sub}$ show the same trend in the flows perturbed by eigenfunctions as in the flows perturbed by random perturbations.

In three-dimensional simulations, vortex pairing is always suppressed by three-dimensional motions and the suppression is greater when the phase difference is larger. Thus the maximum two-dimensional kinetic energy decreases as the phase increases. Three-dimensional motions can grow to sufficient amplitude and eliminate pairing when the phase difference is sufficiently large. Weaker pairing leads to less mixing inasmuch as mixing for the phase of the subharmonic mode of $-\frac{\pi}{2}$ mixing drops more than two times compared to when the phase is 0. The mixing efficiency however diminishes only slightly when the phase changes from 0 to $-\frac{\pi}{2}$ and its value remains close to 0.2, commonly found in previous studies. Mixing sharply decreases as the phase approaches $-\frac{\pi}{2}$, similar to the sharp increase in the time of pairing close to $\pm\frac{\pi}{2}$. These results are consistent with the laboratory observations of Hajj *et al.* [26], and Husain and Hussain [28] for the suppression of the subharmonic mode close to an unfavourable phase.

We examined the effects of the initial amplitude ratio between the KH and subharmonic energy on pairing for the case where the phase was optimal for pairing. We found that by changing the amplitude ratio the time of pairing will be adjusted so that the subharmonic mode reaches the same peak. The changes in the phase of the subharmonic mode however have more significant consequences for the time of pairing as the phase change influences the growth rate of the subharmonic mode. A more comprehensive investigation of the combined effects of the amplitude ratio and the phase is the subject of future studies.

## ACKNOWLEDGMENTS

We are thankful to Dr. Kraig Winters and Dr. Bill Smyth for providing the DNS code and Westgrid for computational resources.

## APPENDIX: AMPLITUDE RATIO EFFECTS

In this Appendix, we examine the effects of the amplitude ratio between the KH and the subharmonic mode of the eigenfunction perturbations in the simulation $E02D$ in Table II. We first lower the amplitude of the initial subharmonic mode to obtain an initial ratio between the kinetic energy of the two modes of $(K_{\rm sub}/K_{\rm kh})_{t_0} = 0.05$. In a second simulation, we increase the amplitude of the subharmonic mode in the initial perturbation to get $(K_{\rm sub}/K_{\rm kh})_{t_0} = 30$. These amplitude ratios are considered to provide significant deviations from one as in natural environments the energy is more likely to be distributed evenly between different modes.

The growth of the kinetic energy of the KH and the subharmonic mode for the three different amplitude ratios are shown in Fig. 10. The KH mode has a higher linear growth rate compared to the subharmonic mode and reaches its first peak around $t = 81$ for all cases. The time evolution of $K_{\rm kh}$ to a saturation is slightly different when $(K_{\rm sub}/K_{\rm kh})_{t_0} = 30$. In all cases, the subharmonic mode exhibits a close to linear growth before reaching a peak at $t_{\rm sub}$. The location of the peak is shifted in time depending on the value of $(K_{\rm sub}/K_{\rm kh})_{t_0}$ and varies between $t_{\rm sub} = 80$ and $t_{\rm sub} = 124$. The growth rates of the subharmonic mode are however the same in all three cases. We also present the trajectories of the fluid particles initially located at vortex centers in Fig. 10. The first crossing of the two particles, that identifies the time of pairing, $t_p$, occurs at $t = 78$ for $(K_{\rm sub}/K_{\rm kh})_{t_0} = 30$ and at $t = 124$ for $(K_{\rm sub}/K_{\rm kh})_{t_0} = 0.05$. These times are summarized in Table III.

The initial amplitude ratio between the KH and the subharmonic mode changes the time of pairing; see Table III. As one might expect, as the initial amplitude of the subharmonic mode relative to the KH mode increases, the time of pairing decreases. However, when compared to the effects of the phase, the amplitude ratio effects are less pronounced. By increasing $(K_{\rm sub}/K_{\rm kh})_{t_0}$ from 0.05 to 30, which is a factor of 600 and an unlikely range of variation in nature, $t_p$ decreases from 125 to

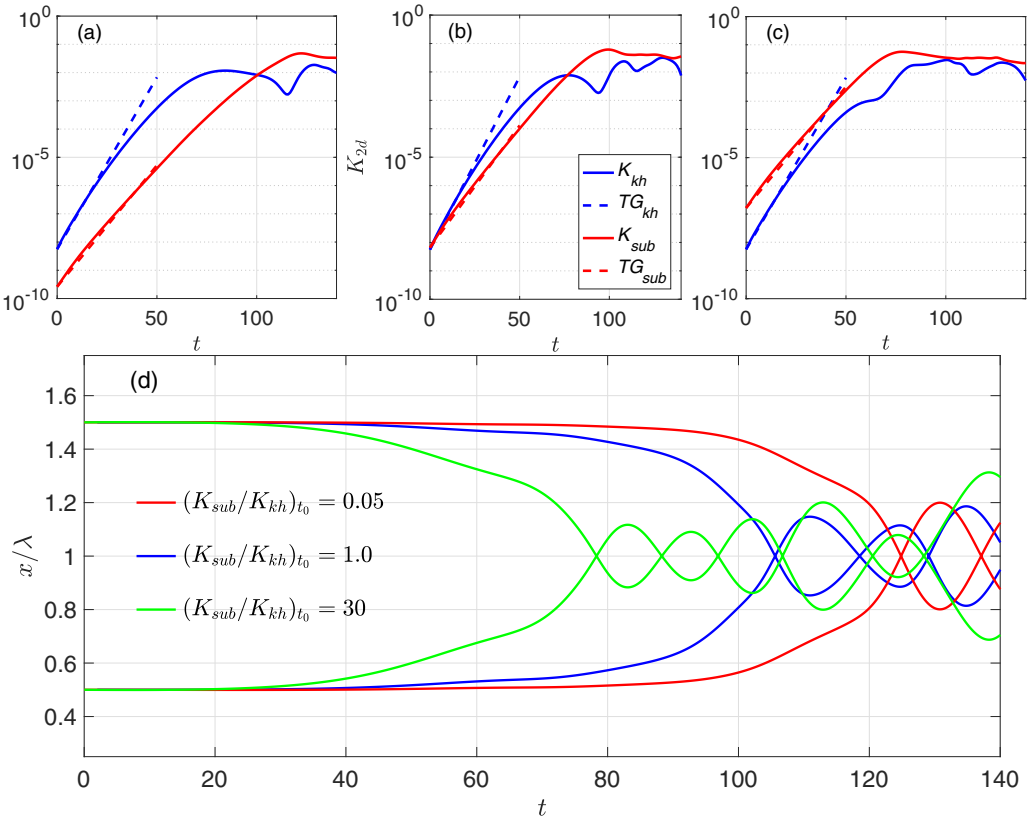


FIG. 10. Effects of the initial perturbation amplitude on the emergence of pairing for the simulation $E02D$. The kinetic energy of the KH and the subharmonic mode for the initial ratios of (a) $(K_{\rm sub}/K_{\rm kh})_{t_0} = 1.0$, (b) $(K_{\rm sub}/K_{\rm kh})_{t_0} = 0.05$, and (c) $(K_{\rm sub}/K_{\rm kh})_{t_0} = 30$. The dashed lines show the linear growth predictions from the Taylor Goldstein equations. Panel (d) shows the $x$ coordinate of two fluid particles initially located at $L_x/4$ and $3L_x/4$.

78. However, for the same simulation, by changing the phase from 0 to $\frac{\pi}{2}$, $t_p$ increases from 107 to 249. The changes in the time of pairing due to the effects of the amplitude ratio are mainly because of the different time required for the subharmonic mode to reach a saturation, while the growth rate of the subharmonic mode remains independent of the amplitude ratio. The phase effects, however, are due to the phase locks between the two modes that occur more slowly and influence the growth rate of the subharmonic mode.

TABLE III. Times of pairing for different initial perturbation amplitude ratios in the simulation $E02D$.

| | $(K_{\rm sub}/K_{\rm kh})_{t_0} = 0.05$ | $(K_{\rm sub}/K_{\rm kh})_{t_0} = 1$ | $(K_{\rm sub}/K_{\rm kh})_{t_0} = 30$ |
|---|---|---|---|
| $t_{\rm sub}$ | 80 | 104 | 124 |
| $t_p$ | 78 | 107 | 125 |

[1] F. K. Browand and C. D. Winant, Laboratory observations of shear-layer instability in a stratified fluid, Boundary-Layer Meteorol. **5**, 67 (1973).
[2] S. A. Thorpe, Experiments on instability and turbulence in stratified shear flow, J. Fluid Mech. **61**, 731 (1973).
[3] C. D. Winant and F. K. Browand, Vortex pairing: The mechanism of turbulent mixing-layer growth at moderate Reynolds number, J. Fluid Mech. **63**, 237 (1974).
[4] W. R. Geyer, A. C. Lavery, M. E. Scully, and J. H. Trowbridge, Mixing by shear instability at high Reynolds number, Geophys. Res. Lett. **37**, L22 (2010).
[5] J. N. Moum and D. M. Farmer, Structure and generation of turbulence at interfaces strained by internal solitary waves propagating shoreward over the continental shelf, J. Phys. Oceanogr. **33**, 2093 (2003).
[6] H. E. Seim and M. C. Gregg, Detailed observations of a naturally occuring shear instability, J. Geophys. Res. **99**, 10049 (1994).
[7] C. P. Caulfield and W. R. Peltier, The anatomy of the mixing transition in homogeneous and stratified free shear layers, J. Fluid Mech. **413**, 1 (2000).
[8] G. P. Klaassen and W. R. Peltier, The effect of Prandtl number on the evolution and stability of Kelvin-Helmholtz billows, Geophs. Astrophys. Fluid Dynamics. **32**, 23 (1985).
[9] A. Mashayek and W. R. Peltier, The "zoo" of secondary instabilities precursory to stratified shear flow transition. Part 1 Shear aligned convection, pairing, and braid instabilities, J. Fluid Mech. **708**, 5 (2012).
[10] A. Mashayek and W. R. Peltier, Shear-induced mixing in geophysical flows: Does the route to turbulence matter to its efficiency? J. Fluid Mech. **725**, 216 (2013).
[11] P. C. Patnaik, F. S. Sherman, and G. M. Corcos, A numerical simulation of Kelvin-Helmholtz waves of finite amplitude, J. Fluid Mech. **73**, 215 (1976).
[12] M. Rahmani, G. A. Lawrence, and B. R. Seymour, The effect of Reynolds number on mixing in Kelvin-Helmholtz billows, J. Fluid Mech. **759**, 612 (2014).
[13] H. Salehipour and W. R. Peltier, Diapycnal diffusivity, turbulent Prandtl number and mixing efficency in Boussinesq stratified turbulence, J. Fluid Mech. **773**, 178 (2015).
[14] C. Staquet, Mixing in a stably stratified shear layer: Two- and three-dimensional numerical experiments, Fluid Dynam. Res. **27**, 367 (2000).
[15] G. M. Corcos and F. S. Sherman, Vorticity concentration and the dynamics of unstable free shear layer, J. Fluid Mech. **73**, 241 (1976).
[16] C.-M. Ho and L.-S. Huang, Subharmonics and vortex pairing in mixing layers, J. Fluid Mech. **119**, 443 (1982).
[17] C. G. Koop and F. K. Browand, Instability and turbulence in a stratified fluid with shear, J. Fluid Mech. **93**, 135 (1979).
[18] G. P. Klaassen and W. R. Peltier, The role of transverse secondary instabilities in the evolution of free shear layers, J. Fluid Mech. **202**, 367 (1989).
[19] A. Mashayek and W. R. Peltier, The "zoo" of secondary instabilities precursory to stratified shear flow transition. Part 2 The influence of stratification, J. Fluid Mech. **708**, 45 (2012).
[20] R. Breidenthal, Structure in turbulent mixing layers and wakes using a chemical reaction, J. Fluid Mech. **109**, 1 (1981).
[21] M. Rahmani, B. Seymour, and G. Lawrence, The evolution of large and small-scale structures in Kelvin-Helmholtz instabilities, Environ. Fluid Mech. **14**, 1725 (2014).
[22] G. M. Corcos and F. S. Sherman, The mixing layer: Deterministic models of a turbulent flow. Part 1. Introduction and the two-dimensional flow, J. Fluid Mech. **139**, 29 (1984).
[23] W. D. Smyth and W. R. Peltier, Two-dimensional turbulence in homogenous and stratified shear layers, Geophs. Astrophys. Fluid Dynam. **69**, 1 (1993).
[24] Chengzhu Xu, Marek Stastna, and David Deepwell, Spontaneous instability in internal solitary-like waves, Phys. Rev. Fluids **4**, 014805 (2019).
[25] R. W. Metcalfe, S. A. Orszag, M. E. Brachet, and J. J. Riley, Secondary instability of a temporally growing mixing layer, J. Fluid Mech. **184**, 207 (1987).
[26] M. R. Hajj, R. W. Miksad, and E. J. Powers, Fundamental–subharmonic interaction: Effect of phase relation, J. Fluid Mech. **256**, 403 (1993).

[27] C.-M. Ho and P. Huerre, Perturbed free shear layers, Annu. Rev. Fluid Mech. **16**, 365 (1984).
[28] H. S. Husain and F. Hussain, Experiments on subharmonic resonance in a shear layer, J. Fluid Mech. **304**, 343 (1995).
[29] S. Kuchibhatla and D. Ranjan, Effect of initial conditions on Rayleigh-Taylor mixing: Modal interaction, Physica Scripta **2013**(T155), 014057 (2013).
[30] S. Goldstein, On the stability of superposed streams of fluids of different densities, Proc. R. Soc. Lond. **132**, 524 (1931).
[31] G. I. Taylor, Effect of variation in density on the stability of superposed streams of fluid, Proc. R. Soc. Lond. **132**, 499 (1931).
[32] P. Hazel, Numerical studies of the stability of inviscid stratified shear flows, J. Fluid Mech. **51**, 39 (1972).
[33] Susan Patricia Haigh, Non-symmetric Holmboe waves, PhD. thesis, University of British Columbia, 1995.
[34] W. D. Smyth and K. B. Winters, Turbulence and mixing in Holmboe waves, J. Phys. Oceanogr. **33**, 694 (2003).
[35] K. B. Winters, J. A. MacKinnon, and B. Mills, A spectral model for process studies of rotating density-stratified flows, J. Atmos. Ocean. Technol. **21**, 69 (2004).
[36] W. D. Smyth, J. D. Nash, and J. N. Moum, Differential diffusion in breaking Kelvin-Helmholtz billows, J. Phy. Oceanogr. **35**, 1004 (2005).
[37] P. Moin and K. Mahesh, Direct numerication simulation: A tool in turbulence research, Annu. Rev. Fluid Mech. **30**, 539 (1998).
[38] G. K. Batchelor, Small-scale variation of convected quantities like temperature in turbulent fluid Part 1. General discussion and the case of small conductivity, J. Fluid Mech. **5**, 113 (1959).
[39] J. R. Carpenter, E. W. Tedford, M. Rahmani, and G. A. Lawrence, Holmboe wave fields in simulation and experiment, J. Fluid Mech. **648**, 205 (2010).
[40] K. B. Winters, P. N. Lombard, J. J. Riley, and E. A. D'asaro, Available potential energy and mixing in density-stratified fluids, J. Fluid Mech. **289**, 115 (1995).
[41] W. D. Smyth and J. N. Moum, Length scales of turbulence in stably stratified mixing layers, Phys. Fluids. **12**, 1327 (2000).
[42] A. K. Kaminski and W. D. Smyth, Stratified shear instability in a field of preexisting turbulence, J. Fluid Mech. **862**, 639 (2019).
[43] A. Mashayek, H. Salehipour, D. Bouffard, C. P. Caulfield, R. Ferrari, M. Nikurashin, W. R. Peltier, and W. D. Smyth, Efficiency of turbulent mixing in the abyssal ocean circulation, Geophys. Res. Lett. **44**, 6296 (2017).
[44] H. Salehipour, C. P. Caulfield, and W. R. Peltier, Turbulent mixing due to the Holmboe wave instability at high Reynolds number, J. Fluid Mech. **803**, 591 (2016).
[45] K. Scharnhorst, Angles in complex vector spaces, Acta Appl. Math. **69**, 95 (2001).
[46] A. Guha and G. A. Lawrence, A wave interaction approach to studying nonmodal homogeneous and stratified shear instabilities, J. Fluid Mech. **755**, 336 (2014).
[47] M. Rahmani, B. R. Seymour, and G. A. Lawrence, The effect of Prandtl number on mixing in low Reynolds number Kelvin-Helmholtz billows, Phys. Fluids. **28**, 054107 (2016).
[48] W. R. Peltier and C. P. Caulfield, Mixing efficiency in stratified shear flows, Annu. Rev. Fluid Mech. **35**, 135 (2003).
[49] W. D. Smyth, J. N. Moum, and D. R. Caldwell, The efficiency of mixing in turbulent patches: Inferences from direct simulations and microstructure observations, J. Phy. Oceanogr. **31**, 1969 (2001).